

Polar Lows over the Nordic Seas: Improved Representation in ERA-Interim Compared to ERA-40 and the Impact on Downscaled Simulations

THIBAUT LAFFINEUR

Ecole Nationale de la Météorologie, Météo-France, Toulouse, and Laboratoire de Météorologie Dynamique/IPSL, CNRS, Ecole Polytechnique, Palaiseau, France

CHANTAL CLAUD

Laboratoire de Météorologie Dynamique/IPSL, CNRS, Ecole Polytechnique, Palaiseau, France

JEAN-PIERRE CHABOUREAU

Laboratoire d'Aérologie, University of Toulouse, and CNRS, Toulouse, France

GUNNAR NOER

The Norwegian Meteorological Institute, Tromsø, Norway

(Manuscript received 28 May 2013, in final form 10 December 2013)

ABSTRACT

Polar lows are intense high-latitude mesocyclones that form during the cold season over open sea. Their relatively small-scale and short life span lead to a rather poor representation in model outputs and meteorological reanalyses. In this paper, the ability of the Interim European Centre for Medium-Range Weather Forecasts (ECMWF) Re-Analysis (ERA-Interim) to represent polar lows over the Norwegian and Barents Sea is assessed, and a comparison with the 40-yr ECMWF Re-Analysis (ERA-40) is provided for three cold seasons (1999–2000 until 2001–02). A better representation in ERA-Interim is found, with 13 systems captured out of the 29 observed, against 6 in the case of ERA-40. Reasons for the lack of representation are identified. Unexpectedly, the representation of different polar low sizes does not appear to be linked to the resolution. Rather, it is the representation of synoptic conditions that appears to be essential. In a second part, a downscaling is conducted using the mesoscale model Meso-NH. For each observed polar low, a pair of simulations is performed: one initialized by ERA-Interim and the other one by ERA-40. An improvement is noted with 22 polar lows represented when ERA-Interim is used. Through a model-to-satellite approach, it is shown that even if polar lows are simulated, convective processes remain insufficiently represented. Wind speeds, which were underestimated in reanalyses, are nevertheless more realistic in the Meso-NH simulations. These results are supported by a spectral analysis of reanalyses and Meso-NH fields.

1. Introduction

Over high-latitude regions of the Northern Hemisphere, intense mesoscale maritime cyclones called “polar lows” (Heinemann and Claud 1997) occasionally occur, mainly during cold season months (from October to May). Despite their small-scale extent (diameter less than 1000 km and thickness of about 1–5 km) and short

life span (few hours to few days), these systems can produce hurricane-like wind gusts and heavy snowfalls (Wilhelmsen 1985). The sudden development of the phenomenon, together with the sparsity of conventional measurements in the genesis and development areas, result in a low forecasting skill (Noer et al. 2011). Therefore polar lows represent a hazard for all maritime and coastal activities (fishing, oil drilling, ...) and population (e.g., West and Hovelsrud 2010).

Generally, polar lows are more frequently observed and more vigorous in the Arctic sector of the North Atlantic Ocean than in the other sectors (e.g., Carleton 1985). In this area, during wintertime, cold-air outbreaks

Corresponding author address: Chantal Claud, Laboratoire de Météorologie Dynamique/IPSL, CNRS, Ecole Polytechnique, Palaiseau 91128, France.
E-mail: chclaud@lmd.polytechnique.fr

may be triggered by the large-scale atmospheric flow exposing dry and very cold air advected over relatively warm water; a situation often conducive to deep convection and polar low formation in the Norwegian and the Barents Seas, which is the focus of this study. Because of the North Atlantic Current (NAC), surface waters in these areas may be warmer than 6°C in winter. These large air-sea temperature differences experienced during cold-air outbreaks result in the formation of atmospheric fronts and sometimes polar lows.

The development of high-resolution satellite image products across a wide range of wavelengths has revealed a variety of mesoscale cyclonic cloud structures associated with polar lows. Indeed, considerable insight into the structure, dynamics, and physics of polar lows has followed advances in remote sensing techniques (e.g., [Claud et al. 1992, 1993, 2009; Bobylev et al. 2011](#)). Observations have revealed a range of conditions leading to the development of such systems, sometimes referred to as the “polar low spectrum” ([Rasmussen and Turner 2003](#)). The striking similarities to tropical hurricanes displayed in some satellite images, such as a clear eye and spiral bands of deep-convective clouds (known as the spiraliform signature), have led several authors to propose the release of latent heat as a major energy source during at least some phases of the polar low life “cycle.” Indeed, past studies proposed two mechanisms to explain convection in polar lows: conditional instability of the second kind (CISK; [Rasmussen 1979](#)), based on latent heat release and wind-induced surface heat exchange (WISHE; [Emanuel and Rotunno 1989](#)), based on low-level fluxes of sensible and latent heat. Other mechanisms like baroclinic instability and upper-level anomalies of potential vorticity also have a major impact on the triggering and the formation of these systems ([Hewson et al. 2000; Yanase and Niino 2007; Bracegirdle and Gray 2008, 2009](#)). Polar lows are phenomena whose dynamical and physical processes may even change a lot during their life cycle; as a consequence, a single polar low may exhibit various cloud signatures, and combine various mechanisms (e.g., [Claud et al. 2004](#)), which make them even more difficult to analyze.

A way to characterize polar lows consists of investigating the synoptic environment in which they develop (e.g., [Claud et al. 2007; Kolstad 2011; Mallet et al. 2013](#)). However, because of their short life span, small size, and occurrence primarily over open ocean, polar lows and their associated environment have been notoriously difficult to study in detail from conventional surface data. With the unprecedented availability over the past decade of high-resolution satellite infrared and microwave observations, it is now possible to directly observe the evolution and structure of polar lows and to assess

the realism of model simulations of these storms (e.g., [Claud et al. 2004; Wagner et al. 2011](#)). Results of the first simulations of polar lows (undertaken in the 1980s) were disappointing because of insufficient horizontal resolution and a poor representation of deep convection. However, significant advances in numerical modeling of polar lows occurred during the subsequent decade. Indeed, in addition to progress in polar low theory (dynamics and physics), improved resolutions (both horizontal and vertical) and a better parameterization of physical processes (deep convection, cloud microphysics, surface fluxes, etc.) have led to more realistic simulations of polar lows. Nowadays, a wide range of mesoscale models, reaching a kilometric-horizontal scale for some, and having both operational and research versions, are used for modeling polar lows (for the most recent studies see [Wu and Petty 2010; Adakudlu and Barstad 2011; Aspelien et al. 2011; McInnes et al. 2011; Nordeng and Røsting 2011; Wagner et al. 2011; Kristiansen et al. 2011; Førre and Nordeng 2012](#), among others).

The characteristics of these systems also present some concerns as to their representation in meteorological reanalyses. [Condron et al. \(2006\)](#) showed that a large portion of these systems is not represented in 40-yr European Centre for Medium-Range Weather Forecasts (ECMWF) Re-Analysis (ERA-40). Although 80% of cyclones larger than 500 km are captured by ERA-40, these authors showed that about 3 out of every 4 polar lows having a size between 100 and 500 km are absent. No comparable study has been conducted with the Interim ECMWF Re-Analysis (ERA-Interim), which has an enhanced spatial resolution of 0.75° (against 1.25° for ERA-40; [Dee et al. 2011](#)). It is expected that the improvements brought to the ERA-Interim reanalysis [four-dimensional variational data assimilation (4D-Var)-improved physical schemes] will lead to a better representation of polar lows compared to ERA-40. One of the first objectives of this paper is precisely to verify the added value afforded by these improvements. To this end, a polar low list compiled mainly from satellite imagery interpreted for the Norwegian and Barents Sea is used (see [Noer et al. 2011](#)). These three databases (polar low dataset, ERA-40, and ERA-Interim) overlap to give 29 polar low cases, observed during three cold seasons from 1999–2000 to 2001–02. Satellite imagery from the Advanced Very High Resolution Radiometer (AVHRR) and Advanced Microwave Sounding Unit-B (AMSU-B) is first used in order to determine polar low principal characteristics (size, life cycle, cloud signatures, and main mechanism of development). Then, the corresponding ERA-40 and ERA-Interim meteorological fields [mean sea level pressure (MSLP), 10-m wind, 500-hPa geopotential height, 850-hPa relative vorticity,

400-hPa potential vorticity, etc.] of each of the 29 cases are examined and compared. Given the relatively small number of polar lows studied here, and to avoid any concerns related to an automatic detection of polar lows, their signatures in reanalyses were manually investigated in plots (presence of a pressure minimum, wind greater or equal to 15 m s^{-1} with a cyclonic rotation and cyclonic vorticity cores).

In a second step, the impacts of a dynamical downscaling procedure and a more adapted representation of the physical mechanisms on the location, the life cycle, and the key variables (like MSLP and low-level wind) for characterizing polar lows are investigated. Accordingly, two sets of Meso-NH simulations are run: one initialized with ERA-Interim and the other one with ERA-40, and the results are compared.

The structure of the paper is as follows. [Section 2](#) describes the data and methods. In [section 3](#) the representation of polar lows in ERA-40 and ERA-Interim is presented, compared, and discussed. In [section 4](#), the added value of Meso-NH simulations as a dynamical downscaling tool for polar low research is investigated. A summary of the results is given in [section 5](#).

2. Data and methods

a. The polar low database

The polar lows dataset specifies the position and time for the first point of detection of a fully developed polar low. The dataset covers the period of late 1999 until the present, and is based on surface sea level pressure analysis made at the Norwegian Meteorological Institute (MET-NORWAY) in Tromsø, Norway ([Noer et al. 2011](#)). Since the area in question is very sparsely covered by synoptic observations, the most important source of information comes from interpretation of the National Oceanic and Atmospheric Administration (NOAA) AVHRR IR images, recently also scatterometer winds, radar, buoys; any other useful information is included in the analysis. Also, in the context of polar lows, the formation process and history up to development is important, in order to distinguish from other similarly looking phenomena. For this, deterministic numerical weather prediction models such as the High Resolution Limited Area Model (HIRLAM) 8- or 12-km model, or the ECMWF operational model are considered. The inventory covers the area from the Greenland east coast to Novaya Zemlya, and from 65°N to the Arctic sea ice edge. In the southwestern corner, the area is also bounded by a line from the northeastern tip of Iceland to Scorsebysund. Wind data are taken from synoptic observations of the past 3-h maximum 10-min 10-m wind,

or from Quick Scatterometer/Advanced Scatterometer (QuikSCAT/ASCAT) retrievals. In this list, dates and positions refer to the time when the low is first identified as a fully developed polar low (i.e., early in the life span of the low). Minimum pressure and maximum wind information are taken from analyses made at MET-NORWAY covering the entire life span of the low. Minimum sea level pressure is taken from synoptic observations or aviation routine weather report (METAR) (airport observations) whenever the low has passed directly over these. If in situ observations are not available, minimum sea level pressure is determined with the aid of an analysis based on model fields, but adjusted to fit the observations. If there is uncertainty on the analysis (e.g., if no observations are available in the vicinity of the center), no data are given. The extreme values in these variables typically occur some 3–9 h after first identification of the polar low. Because of the scarcity of conventional observations, the pressure estimate is approximate, but should be within $\pm 3 \text{ hPa}$.

Most polar lows form in the period November–March with a few cases in October and April–May. We therefore considered the period from October to May as the cold season. The 29 polar lows that occurred during the three study cold seasons (1999–2000, 2000–01, and 2001–02) were analyzed (see [Table 1](#)). With the help of AVHRR infrared images, life span and size estimates of polar lows were determined. The size of polar lows was determined during their mature phase from the AVHRR imagery and is defined as the diameter of the circle formed by the extremities of the cloud vortex, the center of which is the eye of the polar low. Systems are confirmed to be relatively small with more than half of the cases having a diameter less than 300 km ([Figs. 1a–c](#)). Similarly, the short life span of polar lows is confirmed, with only six cases lasting longer than 20 h ([Figs. 1b–d](#)). The geographical distribution of the studied polar lows shows that the largest and longer-lasting systems develop in the Norwegian Sea rather than in the Barents Sea ([Figs. 1a,b](#)). A strong interannual variability is observed: 17 cases formed in the 2001–02 season against only 5 in the 1999–2000 season.

The AVHRR and AMSU-B brightness temperatures allow us to distinguish between convective clouds and low-level cloudiness in polar lows. In the microwave, especially at frequencies higher than 89 GHz, the presence of precipitating hydrometeors leads to lower brightness temperatures because of radiation scattering by large ice particles (e.g., [Chaboureau et al. 2008](#)). Over high-latitude regions, depressed brightness temperatures are frequently observed for convective polar lows with the AMSU-B channel 4 due to its weighting function peaking at 3-km altitude ([Claud et al. 2009](#)). Indeed,

TABLE 1. Main characteristics of the polar lows considered in this study. (column 1) Polar low dates; (column 2) time corresponding to a fully developed low [according to [Noer et al. \(2011\)](#)], (column 3) minimum MSLP reached during the life cycle (hPa) derived from MET-NORWAY analyses; (columns 4–5) minimum MSLP reached during the life cycle (hPa), derived from ERA-40 and ERA-Interim, at H and $H + 6$ (see text for details); (column 6) reanalysis life cycle; (columns 7–8) minimum MSLP reached during the life cycle (hPa), derived from Meso-NH ERA-40 and Meso-NH ERA-Interim, at H and $H + 6$ (see text for details). Here an em dash (—) means no information, \times means no life cycle, \varnothing means no life cycle, NA refers to the case being excluded from the MesoH simulations (see text). D refers to the date of the polar low ($D + 1$: day + 1, etc.). Italics correspond to cases either represented in ERA-Interim, but not in ERA-40, or by Meso-NH ERA-Interim, but not Meso-NH ERA-40.

Day	Hour (UTC)	MSLP _{ana} (hPa)	ERA-40 MSLP _{min} (hPa)	ERA-40 MSLP _{min} (hPa)	ERA-Interim		ERA life cycle	MSLP _{min} (hPa)	Meso-NH MSLP _{min} (hPa)	Meso-NH-E4/ Meso -NH-EI	Meso-NH-E4/ Meso -NH life cycle
					$H + 0/H + 6$	$H + 0/H + 6$					
19 Dec 1999	1340	989	\times/\times	$\times/992$		$\varnothing/1500-2100$ UTC				$\times/994$	$\varnothing/0900$ UTC
22 Jan 2000	0250	990	\times/\times	\times/\times		\varnothing/\varnothing			1002/1000	1500 UTC $D - 1$	1500–1500–1800 UTC $D - 1$
31 Jan 2000	0610	978	\times/\times	\times/\times		\varnothing/\varnothing			082/072	0300–1500/0300–1800 UTC	
8 Mar 2000	1900	992	\times/\times	\times/\times		\varnothing/\varnothing			\times/\times	\varnothing/\varnothing	$\varnothing/0900-2100$ UTC
24 Mar 2000	1230	997	\times/\times	$997/999$		$\varnothing/1200-1800$ UTC			$\times/996$		
1 Jan 2001	1500	—	\times/\times	\times/\times		\varnothing/\varnothing			\times/\times	\varnothing/\varnothing	
4 Feb 2001	1540	—	\times/\times	\times/\times		\varnothing/\varnothing			1002/1002	0600–0000 UTC $D + 1$	0600–0000 UTC $D + 1$
5 Feb 2001	1600	998	$997/995$	$997/993$		$1800-1800$ UTC $D + 1$	$1800-1800-1800$ UTC $D + 1$		984/982	1200–1200 UTC $D + 1$	1200–1200 UTC $D + 1$
2 Mar 2001	0600	—	\ast/\ast			\varnothing/\varnothing			1012/996	0300/0900–0000 UTC $D + 1$	0300/0900–0000 UTC $D + 1$
19 Mar 2001	1400	—	\times/\times			$\varnothing/1200-0000$ UTC $D + 1$			$\times/1008$	$\varnothing/2100-0000$ UTC $D + 1$	$\varnothing/2100-0000$ UTC $D + 1$
24 Mar 2001	0730	1020	\times/\times	\times/\times		\varnothing/\varnothing			$\times/1028$	$\varnothing/0600$ UTC	$\varnothing/0600$ UTC
10 Apr 2001	0650	1000	\times/\times	\times/\times		\varnothing/\varnothing			1002/1008	2100–0000 UTC $D + 1$	2100–0000 UTC $D + 1$
27 Oct 2001	1700	—	1004/1002	998/994		1200–0000 UTC $D + 3$	1200–0000 UTC $D + 3$		996/994	1200–0000 UTC $D + 1$	1200–0000 UTC $D + 1$
1 Nov 2001	0200	992	996/997	996/996		0000–0600/0000–0600 UTC			998/998	0300/0300–0900 UTC	
4 Nov 2001	1900	—	\times/\times	\times/\times		\varnothing/\varnothing			\times/\times	\varnothing/\varnothing	
9 Nov 2001	1700	—	991/990	989/985		0000–0600 UTC $D + 1$	0000–0600–1200 UTC $D + 1$		992/988	1500–2100/0600–0000 UTC $D + 1$	
12 Nov 2001	0700	990	\times/\times	\times/\times		\varnothing/\varnothing			\times/\times	\varnothing/\varnothing	
31 Dec 2001	0400	—	$\times/1003$			1005/1002	1200–0600 UTC $D + 1$	100600–0000 UTC $D + 1$	990/994	0900–0000 UTC $D + 1$	0900–0000 UTC $D + 1$
12 Jan 2002	1200	979	\times/\times	\times/\times		\varnothing/\varnothing			\times/\times	\varnothing/\varnothing	
19 Jan 2002	0400	989	\times/\times	\times/\times		\varnothing/\varnothing			NA/NA	NA/NA	
22 Jan 2002	1100	985	\times/\times	\times/\times		\varnothing/\varnothing			988/984	0300–1800/1500–2100 UTC	
23 Jan 2002	1200	978	980/980	980/980		0600–1800/0600–1800 UTC			984/982	0600–0000 UTC $D + 1$	0600–0000 UTC $D + 1$
26 Jan 2002	0600	—	986/986	984/984		0000 UTC $D - 2$ –0600 UTC $D + 1$ /same			980/980	0600–0000 UTC $D + 1$	0600–0000 UTC $D + 1$
19 Feb 2002	1300	968	\times/\times	\times/\times		\varnothing/\varnothing			\times/\times	\varnothing/\varnothing	
22 Feb 2002	0000	—	\times/\times	\times/\times		\varnothing/\varnothing			980/980	0300/0300–0600 UTC	
23 Feb 2002	1140	958	\times/\times	\times/\times		\varnothing/\varnothing			960/962	1200–0000 UTC $D + 1$	1200–0000–1200–0000 UTC $D + 1$
1 Mar 2002	1200	—	\times/\times	\times/\times		\varnothing/\varnothing			984/980	1500–0000 UTC $D + 1$	1500–0000 UTC $D + 1$
9 Mar 2002	1100	—	\times/\times	\times/\times		\varnothing/\varnothing			$\times/992$	$\varnothing/0600$ UTC $D + 1$	$\varnothing/0600$ UTC $D + 1$
20 May 2002	1436	1010	\times/\times	$1009/\times$		$\varnothing/0600-1200$ UTC			1010/1010	0900–1200/0600–1500 UTC	

* Case is impossible to interpret.

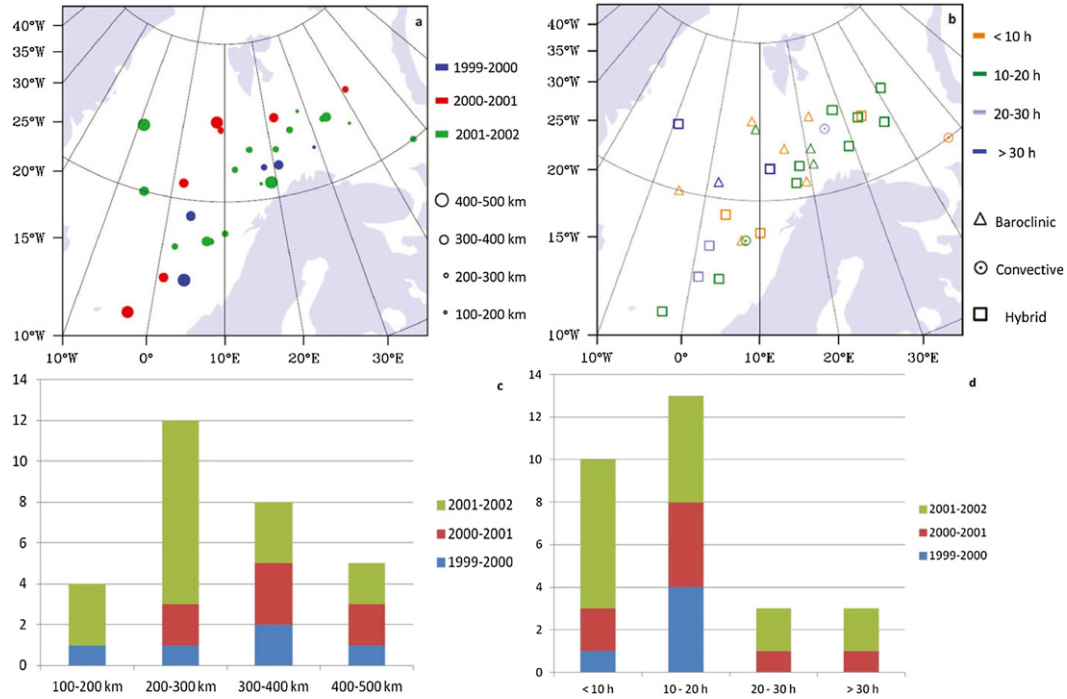


FIG. 1. Summary of characteristics of the 29 polar lows considered in this study: (a) geographical distribution by cold season and diameter, (b) geographical distribution by duration and type, (c) distribution by diameter and cold season, and (d) distribution by duration and cold season.

convective towers reaching into the mid- to upper troposphere are characterized by large hydrometeor contents that scatter the radiation most efficiently. Conversely, lower temperatures for the AMSU-B channel 4 were not observed for baroclinic polar lows (for more details, see [Claud et al. 2009](#)). In the infrared, low brightness temperatures over open ocean characterize high cloud tops, a signature shared by both convective and baroclinic polar lows. Based on these properties, polar lows were classified into three types, as follows: baroclinic, convective, or hybrid (i.e., polar lows that move from baroclinic to convective or reverse at a certain time; see [Fig. 1b](#)). Although most of the cases in our study (60%) are hybrid, a high concentration of baroclinic polar lows is present between Svalbard and northern Norway. Few purely convective polar were observed (three cases).

b. ERA-40 and ERA-Interim reanalyses

Meteorological reanalyses provide a spatially complete, coherent record of the global atmospheric circulation and are not affected by changes in the method used to generate them. We first use the ERA-40 data assimilation system ([Simmons and Gibson 2000](#)), which uses the Integrated Forecast System (IFS) developed jointly by the ECMWF and Météo-France. A three-dimensional variational method assimilates the observations into the

spectral model, which has 60 vertical levels and T159 horizontal spectral resolution. Data are available since 1957 for 23 pressure levels with a spatial resolution of 1.125° . ERA-Interim is the latest ECMWF global atmospheric reanalysis ([Dee et al. 2011](#)). It covers the period 1979 to the present with a 0.75° latitude \times 0.75° longitude grid resolution, and has 37 vertical levels.

Improvements in ERA-Interim relative to ERA-40 include an enhanced spatial resolution, better model physics, improved input datasets and a 4D-Var assimilation scheme. The 4D-Var results in a more effective use of available observations in regions where observations are sparse ([Dee et al. 2011](#)), such as where polar lows develop. One may therefore expect a better representation of polar lows in ERA-Interim compared to its predecessor.

c. Meso-NH simulations

The numerical simulations of the polar lows were made with the nonhydrostatic model Meso-NH ([Lafore et al. 1998](#)) version 4.9. The model was run over a domain of $3072 \text{ km} \times 3072 \text{ km}$ covering the Norwegian and the Barents Seas ([Fig. 12](#)) with a 12-km grid spacing. It includes a mass-flux scheme for deep and shallow convection ([Bechtold et al. 2001](#)), a turbulence parameterization ([Cuxart et al. 2000](#)), a microphysical scheme for

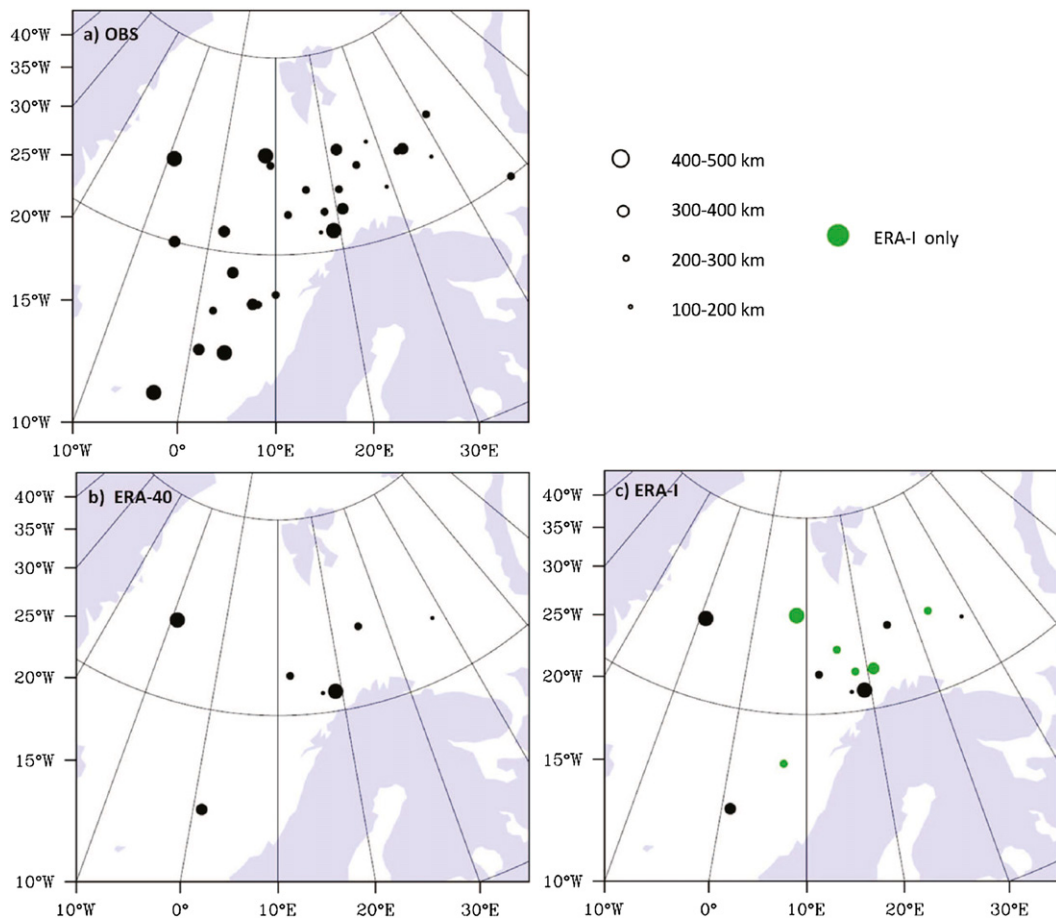


FIG. 2. Location of polar lows in (a) observations (Noer et al. 2011), (b) ERA-40, and (c) ERA-Interim, according to their diameter. Green dots correspond to polar lows detected only in ERA-Interim.

mixed-phase clouds (Pinty and Jabouille 1998), a subgrid statistical cloud scheme (Chaboureau and Bechtold 2002, 2005), and a parameterization for air-sea fluxes (Belamari 2005); all important parameterizations when considering polar low development.

The case of 19 January 2002 (Table 1) was outside the Meso-NH domain, and is excluded from the simulations. Systematic 24-h simulations initiated at 0000 UTC were carried out for the other 28 polar lows, one using initial and lateral boundary conditions provided by ERA-40 and the other one provided by ERA-Interim. In addition, a group of two 36-h simulations (starting at 1200 UTC the day before) was run for polar lows whose mature phase was observed before or close to 0600 UTC. The reasons for this choice are (i) that the time of the onset of the polar low is not known with precision, and (ii) to give sufficient time for the model to accurately simulate the polar low. For each simulation, outputs at 3-hourly intervals were available. The Meso-NH simulated cloud fields were compared with those observed in AVHRR

and AMSU-B using a model-to-satellite approach; such an approach consists of calculating the brightness temperatures at AVHRR and AMSU-B wavelengths using a radiative transfer model [see Clark and Chaboureau (2010) and references therein].

3. Comparison of polar lows represented in ERA-40 and ERA-Interim

a. General results

Minima in MSLP associated with a closed small-scale circulation were used to identify polar lows in the reanalyses. Among the 29 polar lows investigated (Fig. 2a), 13 are represented in ERA-Interim (Fig. 2c) against 7 in ERA-40 (Fig. 2b) (i.e., almost twice as many as in ERA-40). This result was obtained by considering two time steps: H , the synoptic time closest to the time of full development of the PL, and $H + 6$ because of the assumption that PL could be represented with some delay in the reanalyses (Table 1). Indeed one case in ERA-40 (31 December

TABLE 2. Comparison of the polar low main characteristic fields (mean fields) when polar lows are represented in both reanalyses (ERA-40 and ERA-Interim).

Mean fields	ERA-40	ERA-Interim
V_{10m} (m s^{-1})	11.1	14.1
ζ_{850} (10^{-4}s^{-1})	1.3×10^{-4}	1.8×10^{-4}
PV ₄₀₀ (PVU)	3	3
SST – T_{500} ($^{\circ}\text{C}$)	46.5	46.5

2001) and two in ERA-Interim (19 December 1999 and 23 February 2002) fell into this last category. Even though the representation of polar lows is better in ERA-Interim, 16 cases (practically half of the total) remain unrepresented. Figure 2 also shows that some polar lows of relatively small size are represented in reanalyses while some larger ones are missing, suggesting that the horizontal scale of polar lows is not the crucial parameter for their representation in the reanalyses.

The comparison of MSLP fields in ERA-40 and ERA-Interim for polar lows represented in both reanalyses (Table 1) reveals no large difference between ERA-40 and ERA-Interim values, even though systems are generally characterized by a lower MSLP in ERA-Interim. The estimated minimum value of MSLP in both reanalyses is close to the MET-NORWAY analyses provided by Noer et al. (2011), with a mean MSLP error of about 2 hPa. For a few cases, there is an overestimation of MSLP in reanalyses relative to the MET-NORWAY analyses, which could be explained by time differences: polar lows may reach a minimum MSLP at time steps other than H and $H + 6$.

Identification of a polar low in the reanalyses also results in a cyclonic surface wind signature (closed small-scale structure with an anticlockwise circulation). Generally, differences between ERA-40 and ERA-Interim wind fields are small (not shown), but surface wind values in the reanalyses are underestimated compared to usual values measured in polar lows ($11.1\text{--}14.1 \text{ m s}^{-1}$ in reanalyses against 15 m s^{-1} or more by definition; see Table 2).

Examining the relative vorticity fields at 850 hPa reveals, in 24 cases, moderate to high relative vorticity cores near or at the polar low location. Consistently ERA-Interim values are larger than ERA-40 ($1.3 \times 10^{-4} \text{s}^{-1}$ in ERA-40 against $1.8 \times 10^{-4} \text{s}^{-1}$). These intense cores are a signature of the strong cyclonicity accompanying polar lows. But it is important to note that relative vorticity maxima at 850 hPa are not uniquely associated with polar lows, but also with troughs. Consequently, this parameter cannot be used solely for polar low identification and tracking.

To analyze the upper-level dynamics responsible for polar low development, geopotential height at 500 hPa (Z500) and potential vorticity at 400 hPa (PV400) were also investigated. Few differences are found in Z500 fields between the two reanalyses (some troughs were deeper in ERA-Interim), and the synoptic background is clearly favorable to polar low development (presence of troughs, cold air, and surface low areas). We note that for two nonidentified cases, there is a ridge at 500 hPa; hence, a situation prone to large-scale subsidence. In addition, upper-level potential vorticity fields enable us to describe upper-level anomalies, which can be precursors of polar low developments and lead to intensification (e.g., Mallet et al. 2013). In 27 cases, polar lows are associated with a positive anomaly of PV400 (400-hPa potential vorticity) with a mean value about 3 potential vorticity units (PVU, $1 \text{ PVU} = 1 \times 10^{-6} \text{ K kg}^{-1} \text{ m}^2 \text{ s}^{-1}$) in both reanalyses. Among the 13 represented cases, 7 display higher PV400 values in ERA-Interim fields against 3 in ERA-40. As a consequence, where there are high PV400 values, the upper-level anomaly is at lower altitudes, its vorticity field sinks and strengthens cyclonicity at the surface, enabling the polar low to deepen ahead of the trough. This may contribute to the better representation of polar lows in ERA-Interim (see the case of 24 March 2000 below).

The geopotential thickness between the surface and the 500-hPa level (Z1000–Z500) was examined to reveal the presence and strength of a cold air outbreak, considered to be an essential ingredient in polar low formation. In 27 out of 29 cases, a cold air outbreak is present upstream of the polar low in ERA-40 and ERA-Interim fields, with no striking difference between the reanalyses. Finally, the difference between sea surface temperature (SST) and the 500-hPa temperature (T_{500}) is an indicator of convective tropospheric heating driven by surface fluxes in polar lows (Bracegirdle and Gray 2008). In the literature, an SST– T_{500} threshold of $+45^{\circ}\text{C}$ (varying little by region) is considered favorable to polar formation and development. Comparison of the ERA-40 and ERA-Interim fields shows that this threshold is reached in most of the cases, and sometimes even exceeded (46.5°C on average in both reanalyses).

The above results reveal a better representation of polar lows in ERA-Interim than ERA-40. The specific case of 24 March 2000 observed in the Barents Sea ($72^{\circ}\text{N}, 21^{\circ}\text{E}$) (Fig. 3) and only captured in ERA-Interim, is now discussed in order to better describe its synoptic environment in ERA-Interim and illustrate the sensitivity to upper-level anomalies. At 0600 UTC, a PV anomaly moves eastward and begins to interact with a lower-level warm anomaly, increasing cyclonicity in

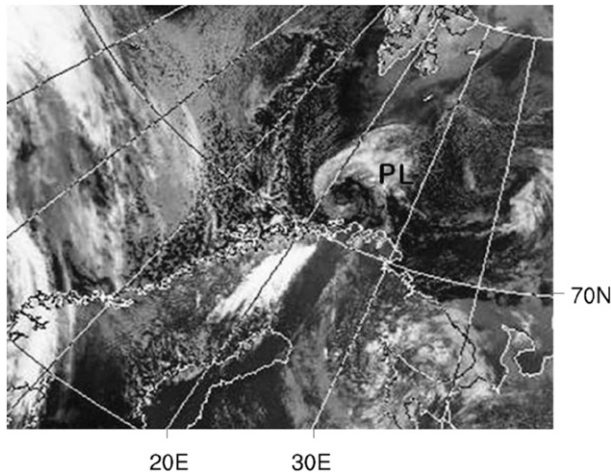


FIG. 3. AVHRR image of the polar low (PL) at 1238 UTC 24 Mar 2000.

the region of the polar low formation. The PV anomaly sinks deeper in the troposphere in ERA-Interim with 3–4 PVU values, but only 2–3 PVU in ERA-40 (not shown). At 1200 UTC, this PV difference between reanalyses is maintained and an MSLP minimum forms in ERA-Interim only (Figs. 4a,b). The maximum in 850-hPa relative vorticity is higher in ERA-Interim ($1.8 \times 10^{-4} \text{ s}^{-1}$) than in ERA-40 ($1.0 \times 10^{-4} \text{ s}^{-1}$). At the surface, air is also slightly warmer in ERA-Interim (4°C) than in ERA-40 (2°C) (Figs. 4c,d). A core of strong vertical velocity is present in ERA-Interim in the polar low area, whereas its amplitude is much weaker in ERA-40 (not shown). Updrafts are better represented in ERA-Interim. Finally, comparing midlevel cloud cover (Figs. 4a,b), ERA-Interim field shows a spiral shape closer to the cloudiness observed in the IR imagery (Fig. 3) than does ERA-40.

b. Polar low trajectories in ERA-40 and ERA-Interim

As shown in Fig. 5, when polar lows are represented in both reanalyses, their trajectories (i.e., tracks of movement) derived from ERA-Interim are spatially closer to the observed trajectories than those derived from ERA-40 (e.g., the case of 27 October 2001). The temporal matching is also better in ERA-Interim. The case of 23 February 2002 also illustrates this point well: this polar low is depicted only once in ERA-40 versus twice in ERA-Interim.

c. Nonrepresented cases

The comparison of MSLP fields in section 3a indicated a better representation of polar lows in ERA-Interim reanalysis. However, more than half of the cases remain unrepresented in both datasets. The more detailed

analysis for the 24 March 2000 polar low has shown that the representation of polar lows in reanalyses is highly sensitive to their synoptic environment.

Considering the whole set of polar lows, three problematic synoptic situations were identified as explaining this poor representation. In the first configuration (10 cases out of 16), the polar low is in the wake of a deeper synoptic-scale depression and we observed that baroclinic processes taking part in polar low formation (i.e., coupling between low- and upper-level anomalies) are poorly represented in favor of the synoptic low. The case of 10 April 2001 at 0600 UTC is discussed now to illustrate this configuration. On the satellite AVHRR image (Fig. 6a), a polar low (PL) is located at 71°N, 2°E on the left flank of a synoptic depression (L) (74°N, 15°E). On Fig. 6b, an MSLP minimum in ERA-Interim is observed in the area of the main low while there is only a trough near the polar low. The spatial phasing between the low-level and altitude anomaly is more efficient for the main low than the polar low. Last, the strong MSLP gradient observed in the polar low area reinforces the northerly winds and prevents the formation of a closed cyclonic circulation. In the second configuration (4 cases out of 16), no MSLP minimum is evident or its geographical position is unstable temporally and not consistent with satellite observations. In the third and least frequent configuration (2 cases out of 16), large-scale subsidence conditions prevail and the polar low is not represented, as in the case of 24 March 2001 (Fig. 7). For this case, there is at the surface a ridge (along 10°E, as shown in Fig. 7, with high pressure decreasing from approximately 80° to 70°N) comprising a range of anticyclonic vorticity values near the region of the polar low (not shown). Cold air, already present in the lowest levels, stabilizes the atmosphere. No interaction between upper-level and lower-level anomalies is possible, which may explain why the polar low is not represented. Last but not least, the two polar lows that fall into this category were both weakly developed vertically. Their formation likely resulted from barotropic instability processes (horizontal shear of jet upstream the upper-level anomaly), as often happens to the west of Svalbard during polar low formation (Rasmussen and Turner 2003).

To conclude this section, even though a strong sensitivity to upper-level and low-level synoptic conditions is observed, one cannot exclude the possibility that the reduced size (diameter $< 200 \text{ km}$) and the short life time ($< 6 \text{ h}$) of a few polar lows play a role in their poor representation in the reanalyses. It is likely that the resolution of both reanalyses is not sufficiently high, and the time step too large, to capture these mesoscale systems.

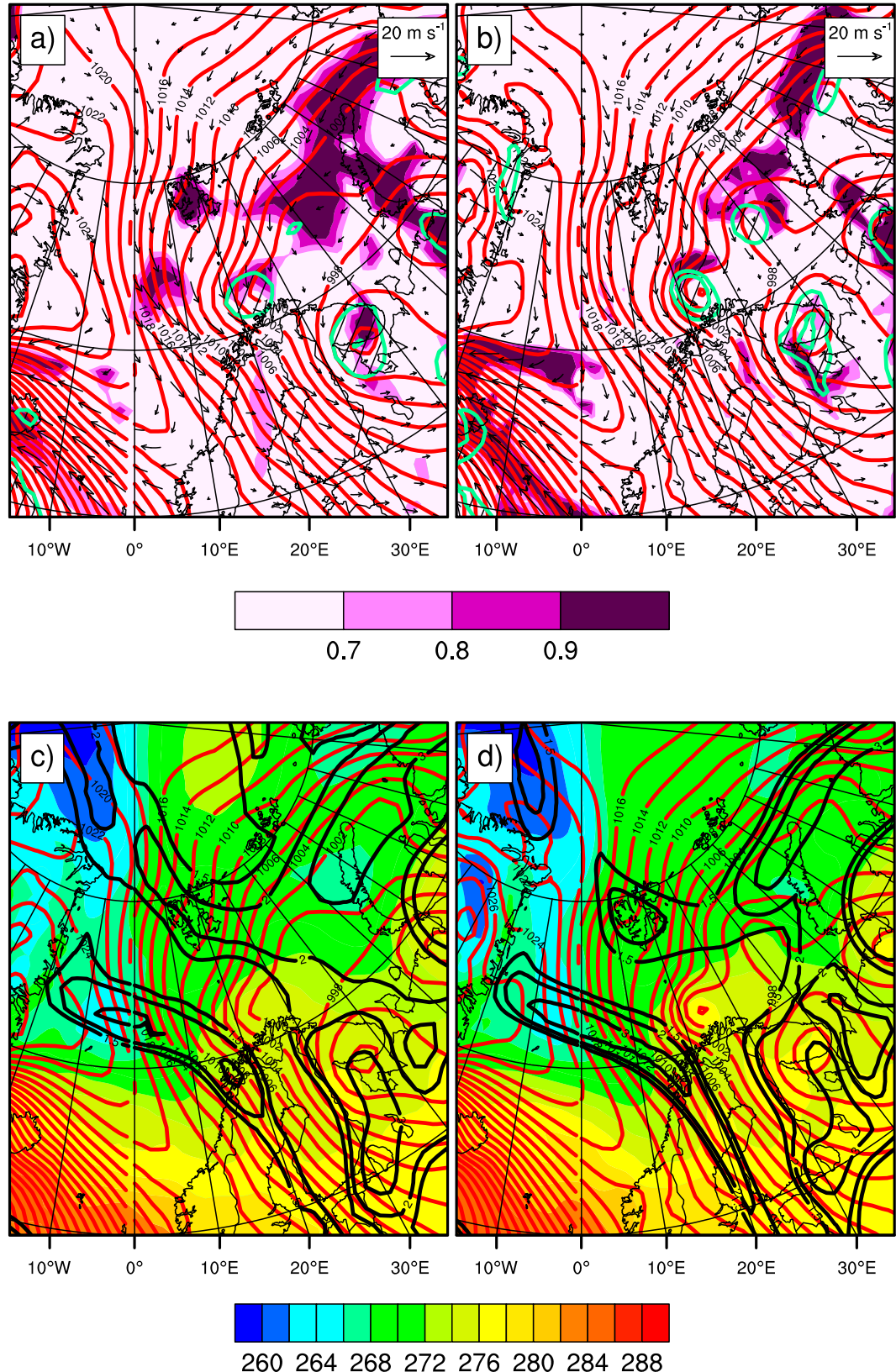


FIG. 4. (a), (c) ERA-40 and (b), (d) ERA-Interim fields valid at 1200 UTC 24 Mar 2000. (a), (b) Midlevel cloud cover (shaded), MSLP (red contours), winds at 10 m (black arrows), and vorticity at 850 hPa (hatched). (c), (d) Potential temperature at 850 hPa (shaded), PV at 400 hPa (black contours), and MSLP (red contours).

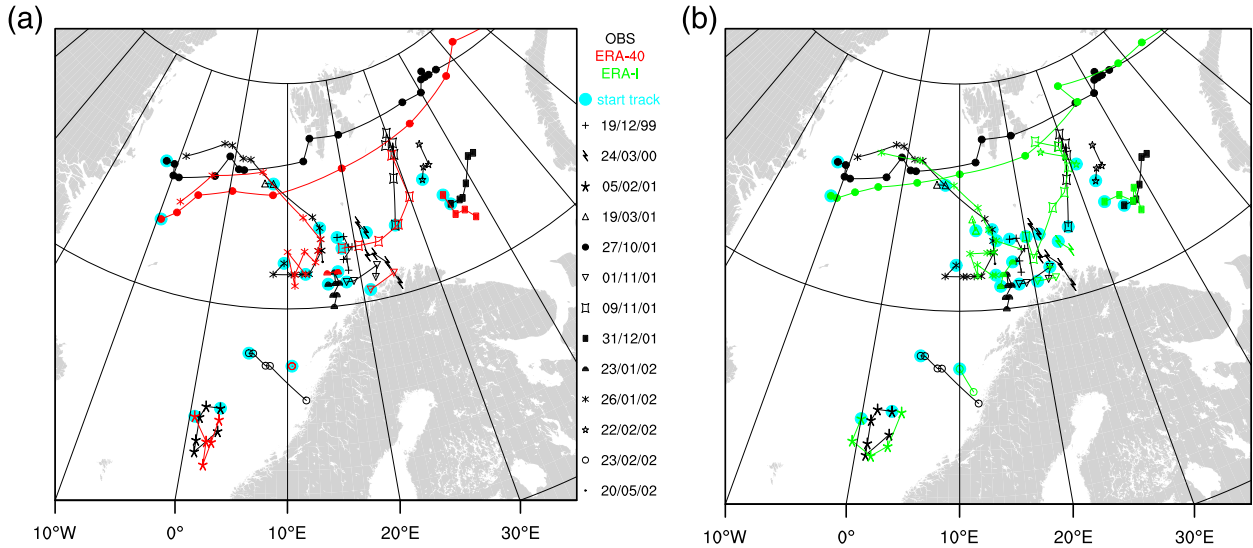


FIG. 5. Polar low trajectories in observations and reanalyses: (a) ERA-40 and (b) ERA-Interim.

4. The added value of Meso-NH simulations

a. General results

The criterion of minima in MSLP identifying polar lows in the reanalyses was also used in the numerical simulations. In total, 22 cases out of 28 were captured by Meso-NH initialized with ERA-Interim (i.e., 9 extra cases vs ERA-Interim; Fig. 8c), and 17 initialized with ERA-40 (i.e., 10 extra cases vs ERA-40; Fig. 8b). Note that three cases are represented after an earlier initialization at 1200 UTC the day before. These results show broadly the positive impact of the mesoscale modeling

on the representation of polar lows. Moreover, the advantage of an initialization with ERA-Interim rather than with ERA-40 is clear (Fig. 8c). Notwithstanding, six cases remain unrepresented. All polar low sizes are equally represented, suggesting again that spatial resolution is not the major factor in successfully representing polar lows, as also suggested in section 3.

As in section 3, a comparison of the main synoptic fields derived from Meso-NH simulations was performed for the types of initialization. As already noted, five cases were not forecast by Meso-NH initialized with ERA-40, but were simulated when initialized with ERA-Interim.

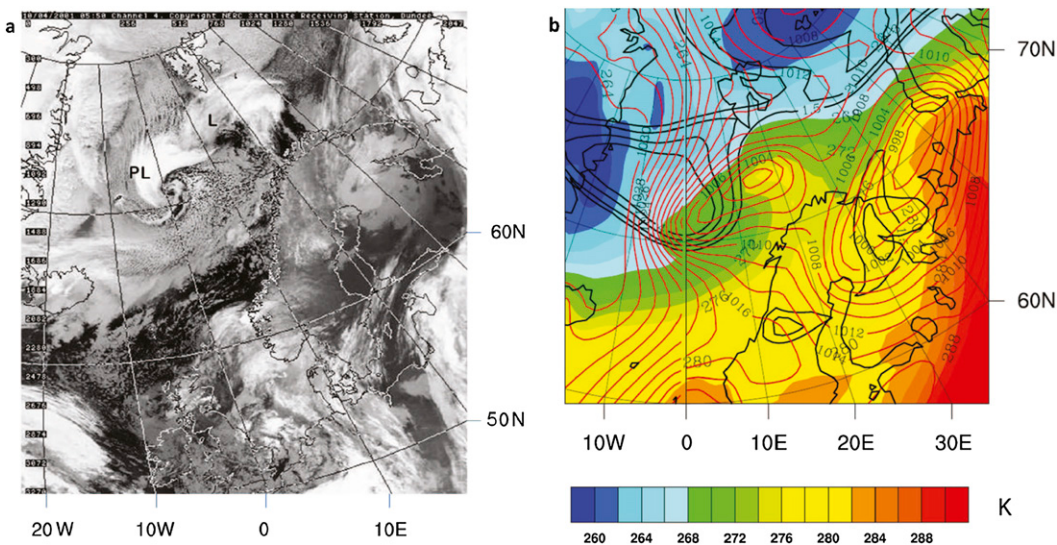


FIG. 6. Polar low of 10 Apr 2001: (a) AVHRR image (0550 UTC) and (b) ERA-Interim (0600 UTC) potential temperature at 850 hPa (K), PV at 400 hPa (black contours), and MSLP (hPa; red contours).

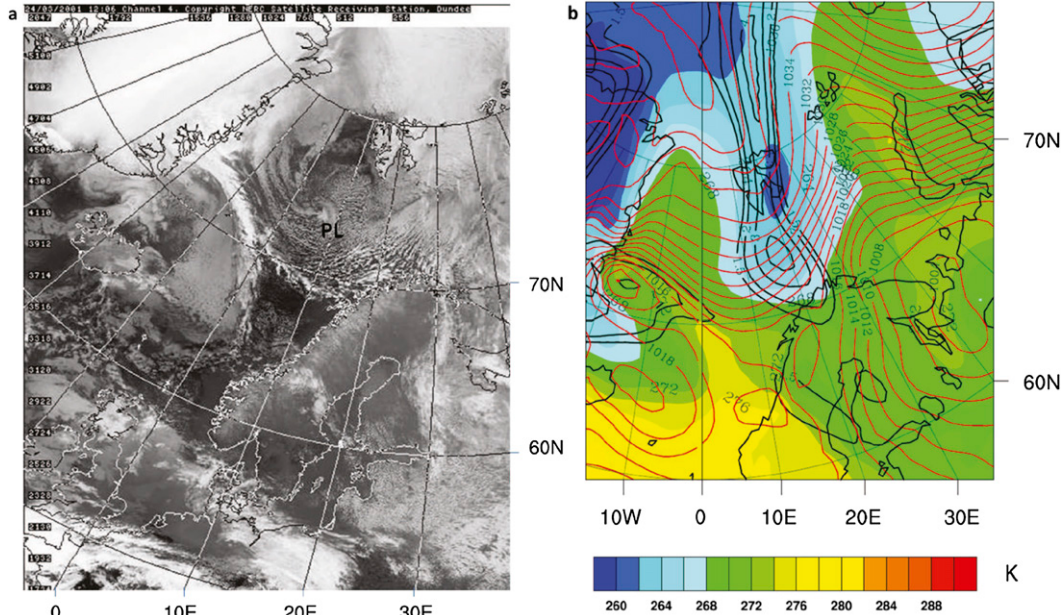


FIG. 7. As in Fig. 6, but at 1208 UTC 24 Mar 2001 for AVHRR and 1200 UTC 24 Mar 2001 for ERA-Interim.

The fact that more cases are represented in the simulations than in the reanalyses shows the advantage of the dynamical downscaling at the finer grid size of 12 km, and that the physics schemes are suitable for representing polar low processes. The comparison of MSLP at the time of lowest sea level pressure (Fig. 9a and Table 1) shows that Meso-NH ERA-Interim tends to deepen polar lows more than Meso-NH ERA-40. Nevertheless, the forecast MSLP shows departures from those analyzed. Only 5 out of 16 forecast MSLP are within 2 hPa and therefore comparable to MET-NORWAY pressures (Noer et al. 2011).

Figure 9b compares the mean maximum 10-m-wind forecast by Meso-NH, initialized by both reanalyses during the polar low life cycle. The strongest 10-m winds are almost all accurately simulated by Meso-NH ERA-Interim, and are typical of the values measured in polar lows (80% reach or exceed the 15 m s^{-1} threshold). In agreement with the results shown by Reistad et al. (2011), an improved representation of wind in polar lows is obtained through use of the dynamical downscaling, here using Meso-NH.

The 850-hPa relative vorticity fields forecast by Meso-NH and initialized by both reanalyses, are highly similar (not shown). Values are often greater than $2 \times 10^{-4} \text{ s}^{-1}$ and underline the strong cyclonicity near the polar low. A comparison of the 400-hPa PV fields highlights the role of PV anomalies for polar low intensification. Indeed, the highest 400-hPa PV values are associated with the deepest polar lows, and the phasing between

upper-level and lower-level anomalies seems to be better represented by Meso-NH (e.g., the case of 31 January 2000, below) than in the reanalyses.

The comparison of observed and simulated AVHRR and AMSU-B4 brightness temperatures associated with polar lows informs the accompanying physical processes. Figure 9c presents the AVHRR 10.8- μm minimum brightness temperature forecast by Meso-NH initialized by ERA-40 and ERA-Interim during the life cycle of polar lows, and Fig. 9d provides the same comparison for AMSU-B4 brightness temperature. Clearly, the lowest temperatures are simulated by Meso-NH initialized by ERA-Interim, even though both Meso-NH ERA-40 and ERA-Interim brightness temperatures are overestimated compared to observations. The Meso-NH ERA-Interim cloudiness is also closer to observations than that of Meso-NH ERA-40. Moreover, in line with observations, convection appears in 14 polar lows at some time during the system's life span and was partly forecast by Meso-NH (not shown). This result indicates that cloudiness and convective activity are better represented in Meso-NH ERA-Interim.

Finally, the convective available potential energy (CAPE) and SST-700 fields are examined. Independent of the initialization, forecast CAPE values are quite low, which may explain the overestimation of the brightness temperatures simulated by Meso-NH. For the surface latent heat fluxes, very few differences are noted between the two simulations (mean value near 150 W m^{-2}). However, this value appears to be underestimated compared

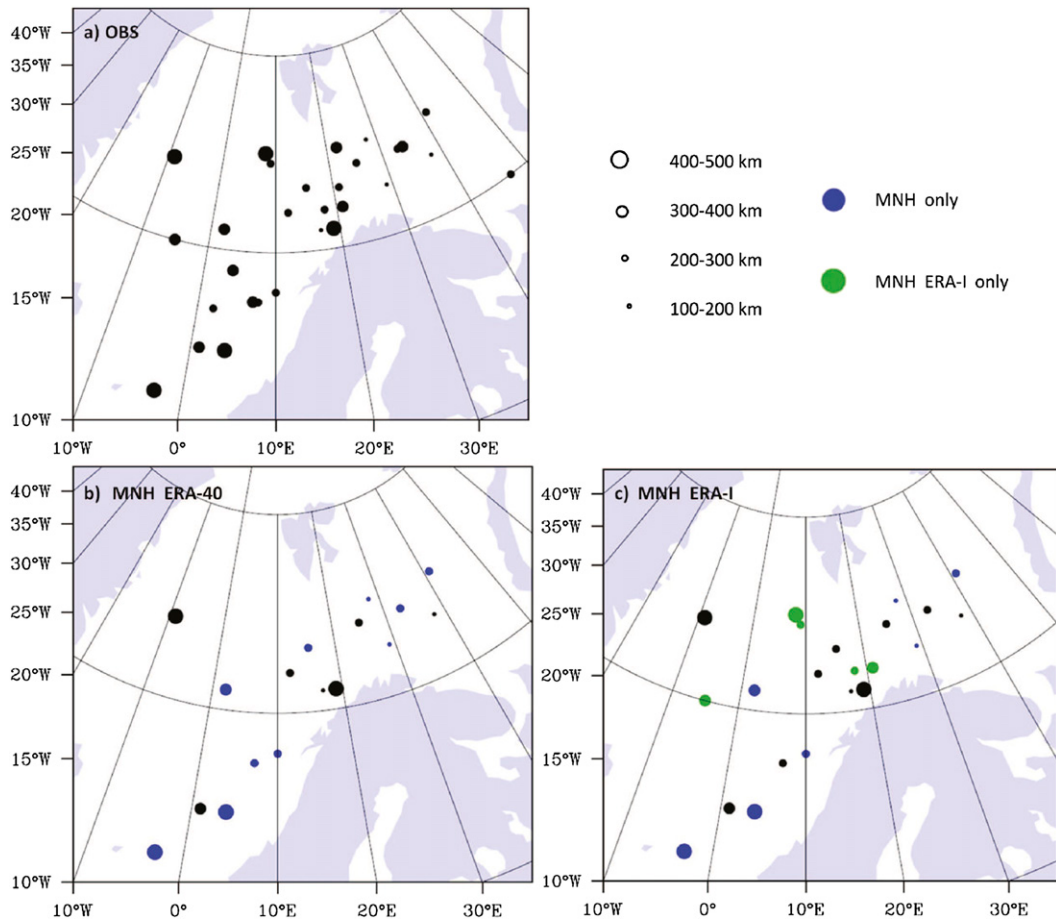


FIG. 8. As in Fig. 2, but for (b) Meso-NH initialized by ERA-40 and (c) Meso-NH initialized by ERA-Interim. Green dots correspond to polar lows detected only in Meso-NH initialized by ERA-Interim.

to the 250 W m^{-2} observed in the polar lows investigated in Blechschmidt (2008).

b. Polar low trajectories in Meso-NH/ERA-40 and ERA-Interim

The polar low trajectories forecast by Meso-NH initialized with ERA-Interim are noticeably closer—both spatially and temporally—to the observed trajectories than those initialized with ERA-40 (e.g., the case of 5 February 2001; Fig. 10). Meso-NH ERA-Interim trajectories often include more points (locations of the polar low at each time step from genesis to dissipation) than Meso-NH ERA-40 (i.e., a total of 101 occurrences against 72). A comparison of the simulated life cycles is given in Fig. 9e (for the onset hours) and Fig. 9f (dissipation hours). Meso-NH ERA-Interim has a tendency to form polar lows earlier than Meso-NH ERA-40. No forecast is totally comparable to the actual observed onset hour. In addition, all Meso-NH ERA-Interim polar lows dissipate later than those in Meso-NH

ERA-40, and no forecast is close to the observed dissipation hours.

c. A further look at specific cases

In this section, specific cases are presented to highlight the results of section 4a, especially in terms of the dynamics and representation of the physical processes. Also, we present further evidence of the added value of Meso-NH for representing polar lows and the advantage of initializing with ERA-Interim (e.g., the case of 31 January 2000), as well as certain limitations (e.g., the case of 24 March 2000).

1) 31 JANUARY 2000

Although absent in the reanalyses, the case of 31 January 2000 is one of the 16 polar lows represented by Meso-NH when initialized with both reanalyses. The Meso-NH ERA-Interim polar low trajectory is more similar to the observation than that in Meso-NH ERA-40, despite a 3-h delay and a too early dissipation. It is

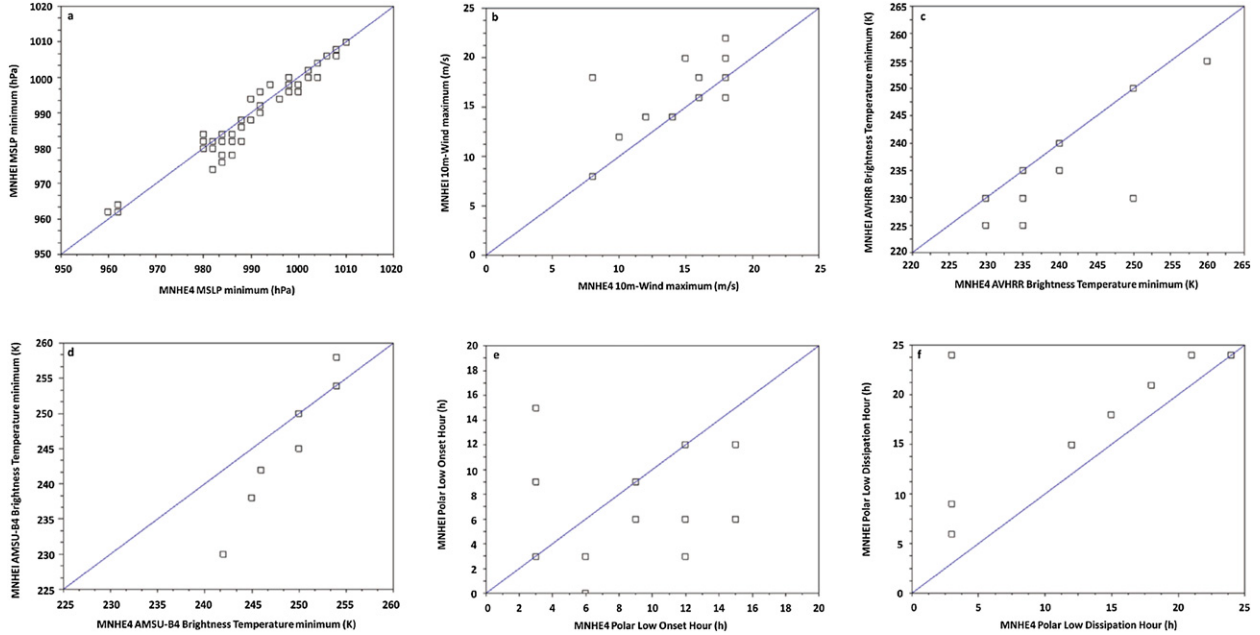


FIG. 9. Comparisons between (a) MSLP, (b) surface wind, (c) minimum AVHRR 10.8- μ m brightness temperature, (d) minimum AMSU-B channel-4 brightness temperature, (e) polar low onset hour, and (f) polar low dissipation time in Meso-NH initialized by ERA-40 and Meso-NH initialized by ERA-Interim.

Meso-NH ERA-Interim that forecasts the lowest MSLP, reaching 978 hPa at 0600 UTC, in agreement with the MET-NORWAY analysis provided by Noer et al. (2011) for the same time.

The interaction between the upper-level PV anomaly and the surface anomaly appears more efficient in the Meso-NH ERA-Interim fields: from 0900 UTC onward, the upper-level anomaly comes closer to the polar low

location, contributing to its fast deepening, which reaches a rate of -1 hPa h^{-1} (Figs. 11a,b). Surface latent heat fluxes are higher in Meso-NH ERA-Interim (200–300 vs 100–150 W m^{-2} in Meso-NH ERA-40); this is true also for surface sensible heat fluxes with more than 300 W m^{-2} in Meso-NH ERA-Interim (not shown). Consequently, low-level convergence and 10-m wind are both stronger in Meso-NH ERA-Interim (not shown).

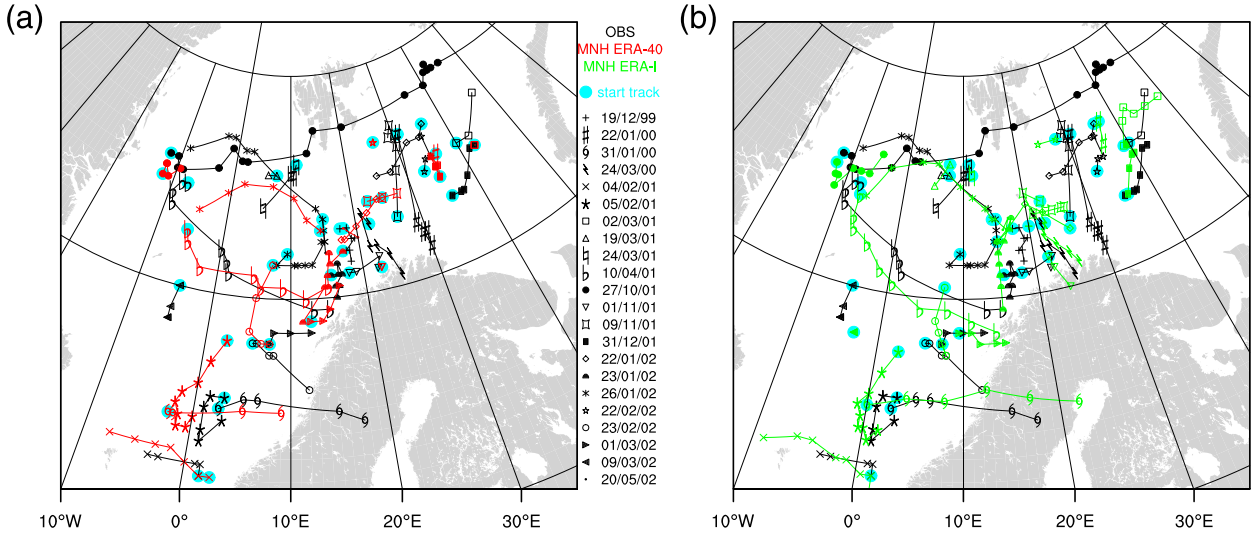


FIG. 10. As in Fig. 5, but for Meso-NH simulations initialized using (a) ERA-40 and (b) ERA-Interim.

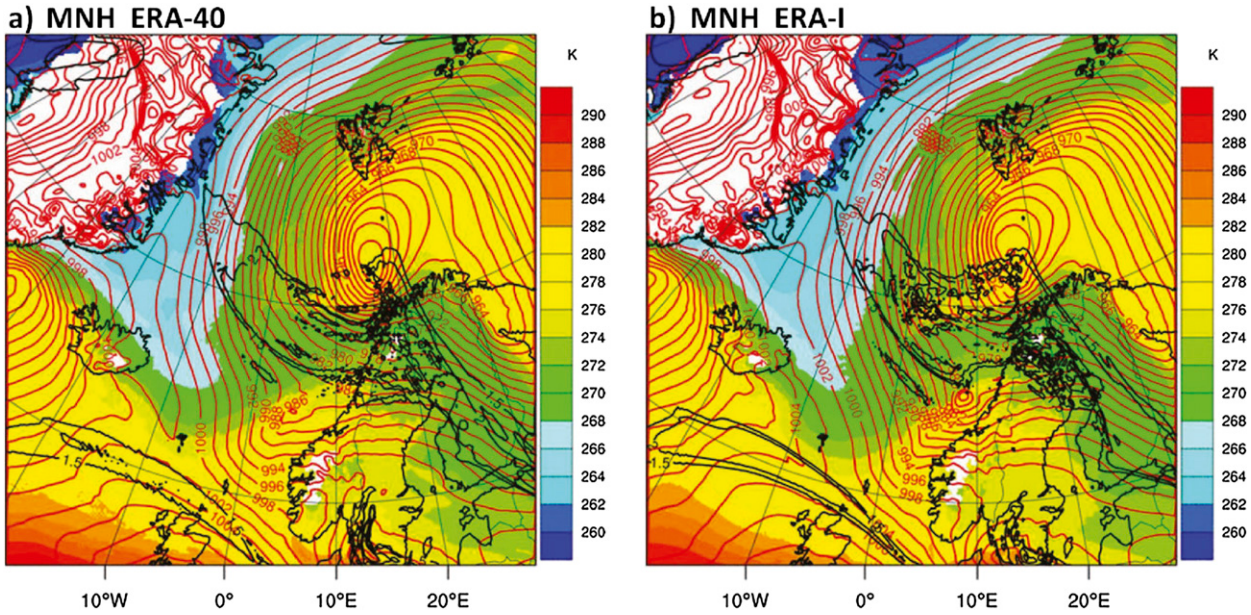


FIG. 11. Comparisons between MSLP, PV at 400 hPa, and potential temperature at 850 hPa in Meso-NH initialized by (a) ERA-40 and (b) ERA-Interim at 0900 UTC 31 Jan 2000.

From 0600 to 1200 UTC—the period of polar low maturity—deep convection appears at 66°N, 9°E (Fig. 12f). Overall Meso-NH simulated brightness temperatures are larger (i.e., less cloud cover, partly because less intense convection is represented) than AVHRR and AMSU-B observations. However, Meso-NH ERA-Interim brightness temperatures are lower than those in Meso-NH ERA-40, indicating that convection is better represented in Meso-NH ERA-Interim.

2) 24 MARCH 2000

In six cases, the dynamical downscaling of Meso-NH does not improve the representation of polar lows, as it is the case for 24 March 2000 (described below).

Only represented in the ERA-Interim reanalysis, the case of 24 March 2000 belongs to polar lows whose representation remains unchanged after the Meso-NH simulations: the polar low is only forecast by Meso-NH initialized with ERA-Interim. That is, the impact of the downscaling can be considered to be neutral. The polar low trajectory agrees quite well with the observations but its formation is delayed (0900 instead of 0100 UTC). As suggested in section 3a, it is possible that upper-level conditions are mainly responsible for this difference of representation. In the Meso-NH ERA-Interim fields, two PV anomalies seem to play a role in the polar low formation (Fig. 13). At the beginning of the life cycle, in the Meso-NH ERA-Interim simulation an upper-level anomaly present over Svalbard sinks to lower altitudes and likely triggers cyclogenesis in the

surface warm air, unlike in Meso-NH ERA-40. Hence, the phasing between upper and lower levels seems better simulated in Meso-NH ERA-Interim. A second upper-level forcing stronger than the first moves eastward and maintains the polar low. Stronger 10-m wind and 850-hPa vertical velocities are simulated by Meso-NH ERA-Interim compared to Meso-NH ERA-40. Moreover, this polar low is marginally convective as displayed by the AVHRR and AMSU-B images (not shown). Hence, the associated brightness temperatures are not very low. The Meso-NH ERA-Interim brightness temperatures are closer to the observations but they remain higher than that observed. Values of the CAPE ($50\text{--}100\text{ J kg}^{-1}$) and SST-T700 (3–5 K) near the polar low confirm that instability is not pronounced in the simulations.

5. Summary and conclusions

Polar lows are intense mesocyclones forming in cold months at high latitudes over open water. Their relatively small-scale and short life time means that they are generally not well represented in model outputs and meteorological reanalysis datasets, as shown by Condron et al. (2006) for the ERA-40 reanalysis. In contrast to the ERA-40 reanalyses, the improvements in ERA-Interim of enhanced spatial resolution, better model physics, improved input datasets, and the 4D-Var assimilation scheme were hypothesized to lead to a better representation of polar lows in ERA-Interim.

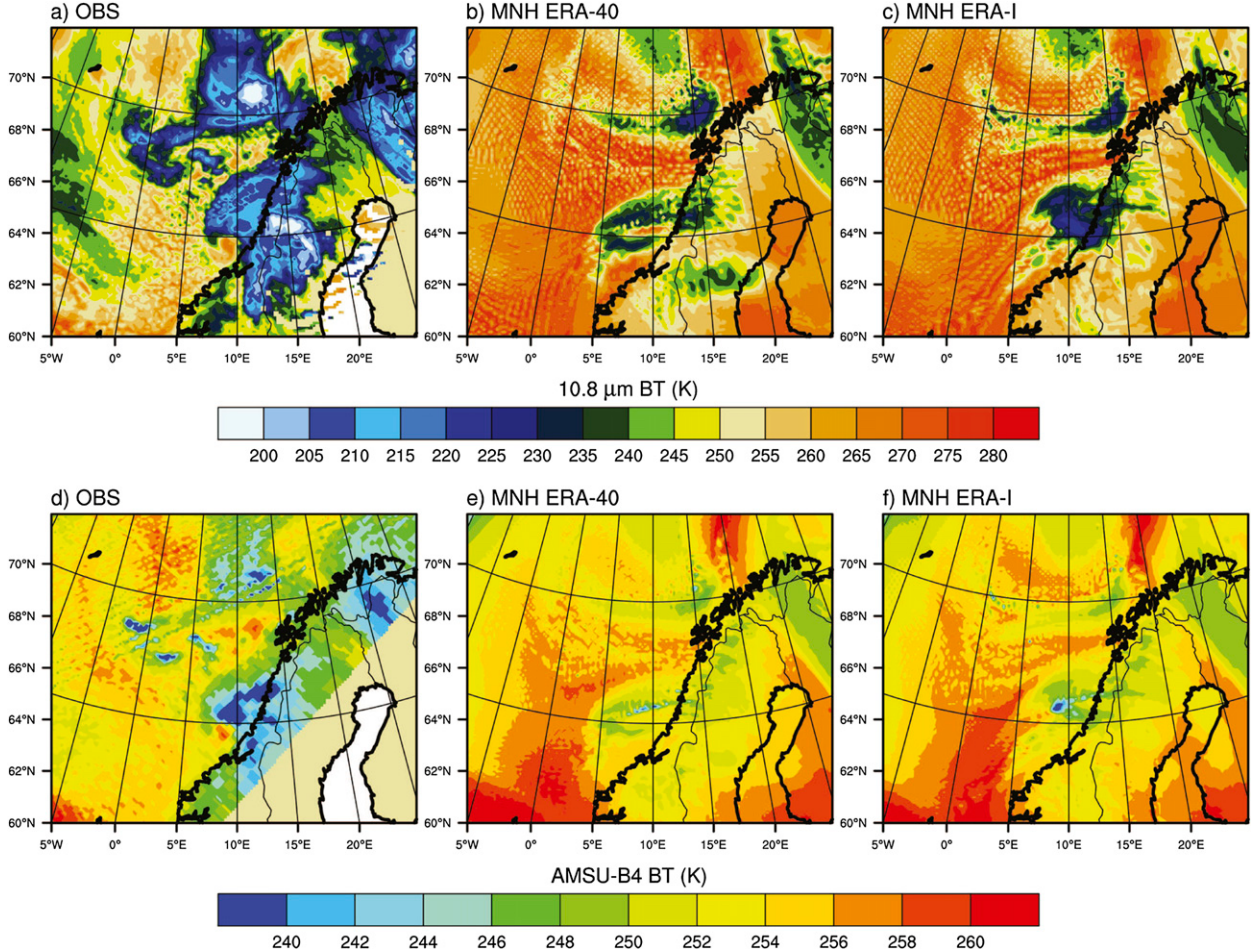


FIG. 12. Comparisons between (a),(d) observed and (b),(c),(e),(f) simulated brightness temperatures at 0900 UTC 31 Jan 2000.

An inventory of polar lows observed over the Norwegian and Barents Seas (Noer et al. 2011) for three consecutive cold seasons has been used as a reference dataset to investigate polar-low representation in the two reanalyses. As expected, the general comparison of meteorological parameters shows a better representation of polar lows in the ERA-Interim reanalysis compared to ERA-40. In mean sea level pressure, 13 polar lows out of 29 observed are represented in ERA-Interim contrasted with only 7 in ERA-40. A consistent result is obtained for the low-level winds. When polar lows are present in the reanalyses, MSLP is comparable to the MET-NORWAY analyses but wind speed is underestimated. Cores of medium to strong relative vorticity are present in almost all cases, with higher values in ERA-Interim. Moreover, upper-level PV anomalies (with higher values in ERA-Interim than in ERA-40) are detected before and during polar low formation. Few differences are noted in geopotential thickness fields (1000–500 hPa), which here is an indicator of cold

air outbreaks, and in SST–T500 fields—an index of static stability—with patterns favorable for polar low development. The polar low life “cycles” and trajectories (i.e., tracks of movement) in ERA-Interim are overall closer to the observations than in ERA-40. Baroclinic processes are found to be more intense in ERA-Interim than ERA-40, which probably explains the better representation of polar lows in ERA-Interim compared to ERA-40. These results are a consequence of a better representation of upper-tropospheric processes in ERA-Interim and the better resolution (not independent of each other), which, added to the improved physical schemes, contribute to a better representation of convection and frontal circulations determinant for polar lows.

When polar lows are not represented in the two reanalyses (16 out of 29), a strong sensitivity to upper and lower synoptic conditions is noted. In a few cases, the reduced size and short life time of polar lows may have played a role. However, we have also identified three situations leading to this poor representation; the most

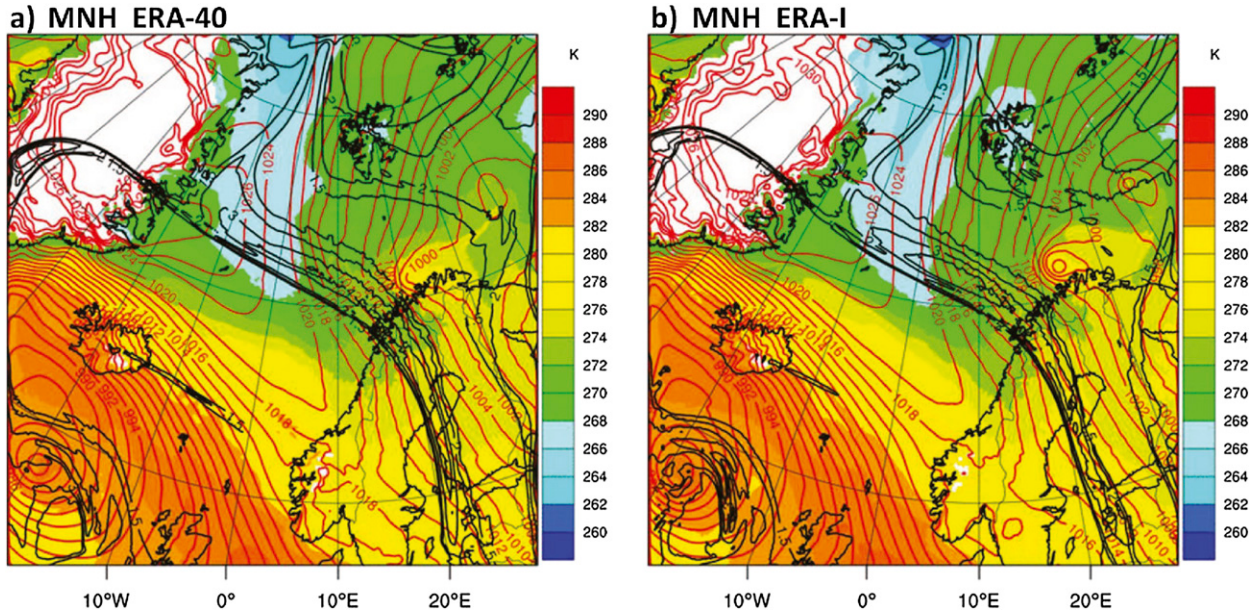


FIG. 13. As in Fig. 11, but at 1500 UTC 24 Mar 2000.

frequent configuration corresponds to a polar low in the wake of a deeper cyclone; in certain other situations, the polar low is masked by a large-scale low pressure area, or to a lesser extent, the synoptic context is anticyclonic and not favorable to polar low formation.

In a complementary second part, Meso-NH simulations of polar lows on a 12-km-grid size and initialized by reanalyses, were analyzed to extract the underlying mechanisms of polar low formation and development. To study the performance of Meso-NH for polar low simulation, a pair of simulations were carried out for each polar low; one initialized with ERA-40 and the other one with ERA-Interim. The Meso-NH simulated cloud fields were compared with those observed, particularly the AMSU-B, using a model-to-satellite approach. Finally, the locations of the simulated polar lows were based on the same criteria as in the reanalyses comparison. Other variables like CAPE, latent, and sensible heat fluxes were explored to better understand the key physical processes in polar lows.

We found that 22 cases out of a total of 28 were represented in Meso-NH when initialized with ERA-Interim, instead of 17 for ERA-40. Within the reanalyses, the representation of different polar low sizes does not appear to be linked with the spatial resolution. Conversely, cases absent from the simulated inventory correspond to situations when the simulated coupling between lower and higher level was not favorable for polar low deepening. An improved representation of surface winds was obtained through the use of Meso-NH. Although there is a clear advantage to using mesoscale modeling

to represent polar lows, deep convection was still underestimated in the simulations; hence, based on model comparisons with the satellite observations, physical processes remain underrepresented.

In line with the studies by Condron and Renfrew (2013) and Ricard et al. (2013), we conducted a spectral analysis for the ERA-40 and ERA-Interim fields that were projected into the Meso-NH grid, as well as for the Meso-NH simulations using the spectral computation developed for the Meso-NH gridpoint fields. It provides compelling support for the results presented in this paper. An example of the spectral analysis is shown in Fig. 14 for the horizontal wind fields in the (left) lower and (right) free troposphere (0–0.5 and 3–6 km, respectively) at 1200 UTC 24 March 2000, associated with a polar low identified only in ERA-Interim and Meso-NH initialized with ERA-Interim fields. In the free troposphere, all the spectra exhibit a k^{-3} dependence on the larger scale. The ERA-40 spectrum departs from the -3 slope at 500 km against 300 km for ERA-Interim. This result indicates that the effective resolution of ERA-40 and ERA-Interim is about 4 times their horizontal resolution. We note that the loss of energy from the 500-km scale in the ERA-40 wind field is consistent with the power spectrum shown by Condron and Renfrew (2013). The spectra for the Meso-NH simulations have more power between 300 and 30 km, showing clearly the added value of the dynamical downscaling. In the low troposphere, all the spectra exhibit a $k^{-5/3}$ dependence on the larger scale due to small-scale phenomena forced by terrain and surface heterogeneities.

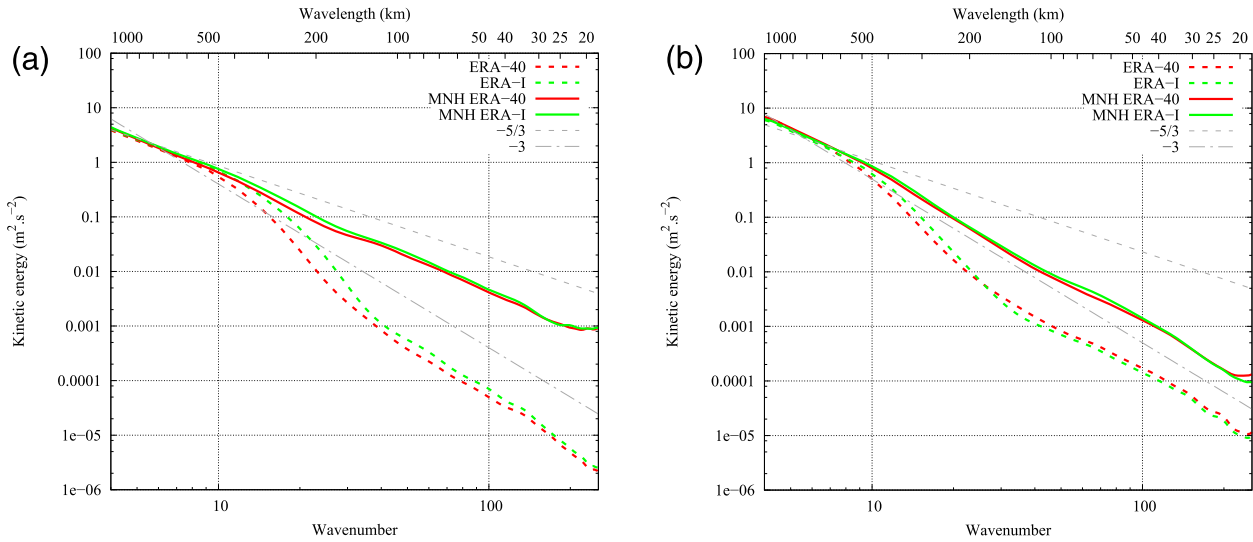


FIG. 14. Power spectra of horizontal wind speed in the (a) lower and (b) free troposphere (0–0.5 and 3–6 km, respectively) over the Nordic Seas for ERA-40, ERA-Interim, as well as Meso-NH ERA-40 and Meso-NH ERA-Interim. Spectra were calculated over the Meso-NH domain at 1200 UTC 24 Mar 2000.

Again, the ERA-40 spectrum departs from the initial slope at a longer scale than ERA-Interim (about 500 vs 300 km). The larger power of the Meso-NH simulations is also very clear. Similar results were obtained for the other polar lows in our study.

Based on this work, the following recommendations concerning polar low research can be made:

- To develop a method for automatically detecting polar lows, caution is required with use of the 850-hPa vorticity, which may be indicative of troughs but not necessarily closed mesocyclonic circulations.
- An impact of polar lows on deep water formation and, hence, in longer-term climate change, has been suggested (Moore et al. 1996; Condron and Renfrew 2013). Condron et al. (2008) have developed an approach that takes account of missing polar lows in reanalyses by imposing surface wind speeds. Our study indicates that even for those polar lows represented in reanalyses, it might be important to adjust wind speeds, because they can be underestimated in the reanalyses, so that the impact of polar lows may indeed be larger than the one noted by Condron and Renfrew (2013).
- Even where using a downscaling approach (e.g., Zahn and van Storch 2008; Zahn et al. 2008), some polar lows remain unrepresented in limited-area models. This means that for deriving polar low climatologies from downscaled reanalyses, it is important to consider a reanalysis in which the representation of polar lows is as faithful to the observations as possible.

Acknowledgments. ERA-Interim and ERA-40 reanalyses were obtained through CLIMSERV. AMSU data were obtained through the French Mixed Service Unit ICARE. TL and CC are grateful to P. E. Mallet and M. Rojo for fruitful discussions. We thank the two anonymous reviewers for their comments on an earlier version of the manuscript. We acknowledge A. M. Carleton for reading the revised manuscript.

REFERENCES

- Adakudlu, M., and I. Barstad, 2011: Impacts of the ice-cover and sea-surface temperature on a polar low over the Nordic seas: A numerical case study. *Quart. J. Roy. Meteor. Soc.*, **137**, 1716–1730, doi:10.1002/qj.856.
- Aspelien, T., T. Iversen, J. B. Bremnes, and I.-L. Frogner, 2011: Short-range probabilistic forecasts from the Norwegian limited-area EPS: Long-term validation and a polar low study. *Tellus*, **63A**, 564–584, doi:10.1111/j.1600-0870.2010.00502.x.
- Bechtold, P., E. Bazile, F. Guichard, P. Mascart, and E. Richard, 2001: A mass-flux convection scheme for regional and global models. *Quart. J. Roy. Meteor. Soc.*, **127**, 869–886, doi:10.1002/qj.49712757309.
- Belamari, S., 2005: Report on uncertainty estimates of an optimal bulk formulation for surface turbulent fluxes. Marine Environment and Security for the European Area-Integrated Project (MERSEA IP), Deliverable D.4.1.2, 29 pp.
- Blechschmidt, A.-M., 2008: A 2-year climatology of polar low events over the Nordic Seas from satellite remote sensing. *Geophys. Res. Lett.*, **35**, L09815, doi:10.1029/2008GL033706.
- Bobylev, L. P., E. V. Zabolotskikh, L. M. Mitnik, and M. L. Mitnik, 2011: Arctic polar low detection and monitoring using atmospheric water vapor retrievals from satellite passive microwave data. *IEEE Trans. Geosci. Remote Sens.*, **49**, 3302–3310, doi:10.1109/TGRS.2011.2143720.

- Bracegirdle, T. J., and S. L. Gray, 2008: An objective climatology of the dynamical forcing of polar lows in the Nordic Seas. *Int. J. Climatol.*, **28**, 1903–1919, doi:10.1002/joc.1686.
- , and —, 2009: The dynamics of a polar low assessed using potential vorticity inversion. *Quart. J. Roy. Meteor. Soc.*, **135**, 880–893, doi:10.1002/qj.411.
- Carleton, A. M., 1985: Satellite climatological aspects of the “polar low” and “instant occlusion.” *Tellus*, **37A**, 433–450, doi:10.1111/j.1600-0870.1985.tb00442.x.
- Chaboureau, J.-P., and P. Bechtold, 2002: A simple cloud parameterization derived from cloud resolving model data: Diagnostic and prognostic applications. *J. Atmos. Sci.*, **59**, 2362–2372, doi:10.1175/1520-0469(2002)059<2362:ASCPDF>2.0.CO;2.
- , and —, 2005: Statistical representation of clouds in a regional model and the impact on the diurnal cycle of convection during Tropical Convection, Cirrus and Nitrogen Oxides (TROCCINOX). *J. Geophys. Res.*, **110**, D17103, doi:10.1029/2004JD005645.
- , and Coauthors, 2008: A midlatitude cloud database validated with satellite observations. *J. Appl. Meteor. Climatol.*, **47**, 1337–1353, doi:10.1175/2007JAMC1731.1.
- Clark, H., and J.-P. Chaboureau, 2010: Uncertainties in short-term forecasts of a Mediterranean heavy precipitation event: Assessment with satellite observations. *J. Geophys. Res.*, **115**, D22213, doi:10.1029/2010JD014388.
- Claud, C., K. B. Katsaros, G. W. Petty, A. Chedin, and N. A. Scott, 1992: A cold air outbreak over the Norwegian Sea observed with the TIROS-N Operational Vertical Sounder (TOVS) and the Special Sensor Microwave Imager (SSM/I). *Tellus*, **44A**, 100–118, doi:10.1034/j.1600-0870.1992.t01-1-00002.x.
- , N. M. Mognard, K. B. Katsaros, A. Chedin, and N. A. Scott, 1993: Satellite observations of a polar low over the Norwegian Sea by Special Sensor Microwave Imager, Geosat, and TIROS-N Operational Vertical Sounder. *J. Geophys. Res.*, **98**, 14 487–14 506, doi:10.1029/93JC00650.
- , G. Heinemann, E. Raustein, and L. McMurdie, 2004: Polar low *le Cygne*: Satellite observations and numerical simulations. *Quart. J. Roy. Meteor. Soc.*, **130**, 1075–1102, doi:10.1256/qj.03.72.
- , B. Duchiron, and P. Terray, 2007: Associations between large-scale atmospheric circulation and polar low developments over the North Atlantic during winter. *J. Geophys. Res.*, **112**, D12101, doi:10.1029/2006JD008251.
- , B. M. Funatsu, G. Noer, and J.-P. Chaboureau, 2009: Observation of polar lows by the Advanced Microwave Sounding Unit: Potential and limitations. *Tellus*, **61A**, 264–277, doi:10.1111/j.1600-0870.2008.00384.x.
- Condron, A., and I. A. Renfrew, 2013: The impact of polar mesoscale storms on northeast Atlantic Ocean circulation. *Nat. Geosci.*, **6**, 34–37, doi:10.1038/ngeo1661.
- , G. R. Bigg, and I. A. Renfrew, 2006: Polar mesoscale cyclones in the Northeast Atlantic: Comparing climatologies from ERA-40 and satellite imagery. *Mon. Wea. Rev.*, **134**, 1518–1533, doi:10.1175/MWR3136.1.
- , —, and —, 2008: Modeling the impact of polar mesocyclones on ocean circulation. *J. Geophys. Res.*, **113**, C10005, doi:10.1029/2007JC004599.
- Cuxart, J., P. Bougeault, and J.-L. Redelsperger, 2000: A turbulence scheme allowing for mesoscale and large-eddy simulations. *Quart. J. Roy. Meteor. Soc.*, **126**, 1–30, doi:10.1002/qj.49712656202.
- Dee, D. P., and Coauthors, 2011: The ERA-Interim reanalysis: Configuration and performance of the data assimilation system. *Quart. J. Roy. Meteor. Soc.*, **137**, 553–597, doi:10.1002/qj.828.
- Emanuel, K. A., and R. Rotunno, 1989: Polar lows as arctic hurricanes. *Tellus*, **41A**, 1–17, doi:10.1111/j.1600-0870.1989.tb00362.x.
- Føre, I., and T. E. Nordeng, 2012: A polar low observed over the Norwegian Sea on 3–4 March 2008: High-resolution numerical experiments. *Quart. J. Roy. Meteor. Soc.*, **138**, 1983–1998, doi:10.1002/qj.1930.
- Heinemann, G., and C. Claud, 1997: Report of a workshop on “Theoretical and observational studies of polar lows” of the European Geophysical Society Polar Lows Working Group. *Bull. Amer. Meteor. Soc.*, **78**, 2643–2658.
- Hewson, T. D., G. C. Craig, and C. Claud, 2000: Evolution and mesoscale structure of a polar low outbreak. *Quart. J. Roy. Meteor. Soc.*, **126**, 1031–1063, doi:10.1002/qj.49712656411.
- Kolstad, E. W., 2011: A global climatology of favourable conditions for polar lows. *Quart. J. Roy. Meteor. Soc.*, **137**, 1749–1761, doi:10.1002/qj.888.
- Kristiansen, J., S. L. Sorland, T. Iversen, D. Bjorge, and M. Ø. Koltzow, 2011: High-resolution ensemble prediction of a polar low development. *Tellus*, **63A**, 585–604, doi:10.1111/j.1600-0870.2010.00498.x.
- Lafore, J.-P., and Coauthors, 1998: The Meso-NH Atmospheric Simulation System. Part I: Adiabatic formulation and control simulations. *Ann. Geophys.*, **16**, 90–109, doi:10.1007/s00585-997-0090-6.
- Mallet, P.-E., C. Claud, C. Cassou, G. Noer, and K. Kodera, 2013: Polar lows over the Nordic and Labrador Seas: Synoptic circulation patterns and associations with North Atlantic–Europe wintertime weather regimes. *J. Geophys. Res.*, **118**, 2455–2472, doi:10.1002/jgrd.50246.
- McInnes, H., J. Kristiansen, J. E. Kristjánsson, and H. Schyberg, 2011: The role of horizontal resolution of polar low simulations. *Quart. J. Roy. Meteor. Soc.*, **137**, 1674–1687, doi:10.1002/qj.849.
- Moore, G. W. K., M. C. Reader, J. York, and S. Sathyamoorthy, 1996: Polar lows in the Labrador Sea. *Tellus*, **48A**, 17–40, doi:10.1034/j.1600-0870.1996.00002.x.
- Noer, G., Ø. Sætra, T. Lien, and Y. Gusdal, 2011: A climatological study of polar lows in the Nordic Seas. *Quart. J. Roy. Meteor. Soc.*, **137**, 1762–1772, doi:10.1002/qj.846.
- Nordeng, T. E., and B. Røsting, 2011: A polar low named Vera: The use of potential vorticity diagnostics to assess its development. *Quart. J. Roy. Meteor. Soc.*, **137**, 1790–1803, doi:10.1002/qj.886.
- Pinty, J.-P., and P. Jabouille, 1998: A mixed-phase cloud parameterization for use in mesoscale non-hydrostatic model: Simulations of a squall line and of orographic precipitation. *Preprints, Conf. on Cloud Physics*, Everett, WA, Amer. Meteor. Soc., 217–220.
- Rasmussen, E. A., 1979: The polar low as an extratropical CISK disturbance. *Quart. J. Roy. Meteor. Soc.*, **105**, 531–549, doi:10.1002/qj.49710544504.
- , and J. Turner, 2003: *Polar Lows: Mesoscale Weather Systems in the Polar Regions*. Cambridge University Press, 612 pp.
- Reistad, M., Ø. Breivik, H. Haakenstad, O. J. Aarnes, B. R. Furevik, and J.-R. Bidlot, 2011: A high-resolution hindcast of wind and waves for the North Sea, the Norwegian Sea, and the Barents Sea. *J. Geophys. Res.*, **116**, C05019, doi:10.1029/2010JC006402.
- Ricard, D., C. Lac, S. Riette, R. Legrand, and A. Mary, 2013: Kinetic energy spectra characteristics of two convection-permitting limited-area models AROME and Meso-NH.

- Quart. J. Roy. Meteor. Soc.*, **139**, 1327–1341, doi:10.1002/qj.2025.
- Simmons, A. J., and J. K. Gibson, 2000: The ERA-40 Project Plan. ERA-40 Project Rep. Series 2000, Rep. 1, ECMWF, Reading, United Kingdom, 63 pp.
- Wagner, J. S., A. Gohm, A. Dörnbrack, and A. Schäfler, 2011: The mesoscale structure of a polar low: Airborne lidar measurements and simulations. *Quart. J. Roy. Meteor. Soc.*, **137**, 1516–1531, doi:10.1002/qj.8571.
- West, J. J., and G. K. Hovelsrud, 2010: Cross-scale adaptation challenges in the coastal fisheries: Findings from Lebesby, Northern Norway. *Arctic*, **63**, 338–354, doi:10.14430/arctic1497.
- Wilhelmsen, K., 1985: Climatological study of gale-producing polar lows near Norway. *Tellus*, **37A**, 451–459, doi:10.1111/j.1600-0870.1985.tb00443.x.
- Wu, L., and G. W. Petty, 2010: Intercomparison of bulk micro-physics schemes in model simulations of polar lows. *Mon. Wea. Rev.*, **138**, 2211–2228, doi:10.1175/2010MWR3122.1.
- Yanase, W., and H. Niino, 2007: Dependence of polar low development on baroclinicity and physical processes: An idealized high-resolution numerical experiment. *J. Atmos. Sci.*, **64**, 3044–3067, doi:10.1175/JAS4001.1.
- Zahn, M., and H. von Storch, 2008: A long-term climatology of North Atlantic polar lows. *Geophys. Res. Lett.*, **35**, L22702, doi:10.1029/2008GL035769.
- , —, and S. Bakan, 2008: Climate mode simulation of North Atlantic polar lows in a limited area model. *Tellus*, **60A**, 620–631, doi:10.1111/j.1600-0870.2008.00330.x.